

# A Sparse Expansion For Deep Gaussian Processes

Liang Ding<sup>a</sup>, Rui Tuo<sup>b</sup> and Shahin Shahrampour<sup>c</sup>

<sup>a</sup> School of Data Science, Fudan University, Shanghai, China

<sup>b</sup> Industrial & Systems Engineering, Texas A&M University, College Station, TX

<sup>c</sup> Mechanical & Industrial Engineering, Northeastern University, Boston, MA

## Abstract

In this work, we use Deep Gaussian Processes (DGPs) as statistical surrogates for stochastic processes with complex distributions. Conventional inferential methods for DGP models can suffer from high computational complexity as they require large-scale operations with kernel matrices for training and inference. In this work, we propose an efficient scheme for accurate inference and efficient training based on a range of Gaussian Processes, called the *Tensor Markov Gaussian Processes* (TMGP). We construct an induced approximation of TMGP referred to as the *hierarchical expansion*. Next, we develop a deep TMGP (DTMGP) model as the composition of multiple hierarchical expansion of TMGPs. The proposed DTMGP model has the following properties: (1) the outputs of each activation function are deterministic while the weights are chosen independently from standard Gaussian distribution; (2) in training or prediction, only  $\mathcal{O}(\text{polylog}(M))$  (out of  $M$ ) activation functions have non-zero outputs, which significantly boosts the computational efficiency. Our numerical experiments on synthetic models and real datasets show the superior computational efficiency of DTMGP over existing DGP models.

*Keywords:* deep Gaussian processes; Markov Gaussian processes; inducing variables; sparse expansion.

## 1 Introduction

This work is partially motivated by surrogate modeling of stochastic computer simulations (Ankenman et al., 2010; Plumlee and Tuo, 2014). The ultimate goal in this field is to approximate an underlying stochastic process, defined by a complex stochastic computer simulation code, using a surrogate stochastic process that is computationally efficient. Among existing statistical surrogates, Deep Gaussian Processes (DGP) proposed by Damianou and Lawrence (2013) has recently become a popular choice owing to its exceptional performance and flexibility in fitting the complex distributions from the stochastic processes in real applications (Radaideh and Kozlowski, 2020; Sauer et al., 2022).

DGPs are multi-layer compositions of multi-variate Gaussian Processes (GP). The deep probabilistic structures of DGPs allows a Bayesian formulation to model complex stochastic systems, such as computer vision, natural language processing, etc.. However, the cost of DGPs’ expressiveness and flexibility is the extreme difficulties in training and inference, because the propagation of randomness throughout the layers of DGPs is nonlinear and correlated among layers. Existing approaches for overcoming these difficulties can be separated into two classes – one class focuses on approximating the Bayesian formulations of DGPs, such as variational inference (VI) (Blei et al., 2017), expectation propagation (EP) (Bui et al., 2016), or Vecchia approximation (Sauer et al., 2022a), while the other class considers simplified representations of DGPs’ structures, such as inducing-variable approximation (Hensman and Lawrence, 2014) and random Fourier feature expansion (Cutajar et al., 2017).

Simplifications based on inducing variables and random Fourier features (Rahimi and Recht, 2008) partially address the computational issue of DGPs. However, they are still hard to implement. This is because these simplifications of DGPs are deep Neural Networks (DNN) with kernel based activations, correlated random weights and bias parameters, which is equivalent to Bayesian Neural Networks (BNN) (MacKay, 1992; Neal, 1996) with dense and highly correlated structures. Training and inference of these simplifications are at least as hard as existing BNN models.

In this work, we focus on introducing an accurate and efficient simplification of DGPs. We propose a sparse reduced-rank approximation, referred as *Hierarchical Expansion*, for DGPs. Our expansion is specialized for DPGs which are the compositions of multi-variate tensor Markov GPs (TMGP) (Ding and Zhang, 2020), so we call this expanded DGP deep TMGP (DTMGP). One of our main contributions lies in constructing a sparse representation of DGPs. There are only a poly-logarithmic number of activations in our model with non-zero outputs each time we run the model. Because of this sparse property, training of DTMGPs are much faster and easier compared with existing DGP models, avoiding commonly seen numerical issues in training deep models. Another contribution is to show that hierarchical expansion is also highly accurate. Unlike many other GPs/DGPs sparse approximations, the difference between sample paths generated by any DGP and those generated by its hierarchical expansion is small. This property allows DTMGPs to model complex stochastic

systems with satisfactory performance as shown in our numerical experiments.

We use VI to train DTMGP on data generated from simulations and real data and compare it with other existing DGP models. We conduct simulation studies by running experiments on an artificial random field and simulator of a stochastic activity network (Pasupathy and Henderson, 2011). We also use the RC-49 data set, which is publicly available on the web <https://paperswithcode.com/dataset/rc-49>, to demonstrate the performance of the proposed approach. In these numerical studies, we find that the training process of DTMGP is more stable, and the training loss converges faster compared with its competitors. Besides, we compare the similarities between instances from the underlying systems and instances generated from competing statistical surrogate models. The results show that DTMGP outperforms the alternative DGPs in all experiments.

The remainder of this article is organized as follows. We will review the related literature in Section 2. We introduce general DGP models and an approximation of DGPs called induced approximation in Section 3. The methodology and detailed implementation of DTMGP are introduced in Section 4. Simulation studies are given in Section 5 and experiments on real data are given in 6 . Concluding remarks are made in Section 7. The Appendix includes the required mathematical tools and technical proofs.

## 2 Literature Review

The state-of-the-art deep learning techniques have brought probabilistic modeling with deep neural network structure in popularity. Based on the concept of deep belief network (DBN) (Hinton et al., 2006), Damianou and Lawrence (2013) generalized the Restricted Boltzmann Machine (Hinton, 2010), which is a DBN with binary output, to deep Gaussian Processes based on Gaussian process mapping. DGPs have been a popular tool in several applications. Their prowess has been demonstrated on many classification tasks (Damianou and Lawrence, 2013; Fei et al., 2018; Yang and Klabjan, 2021). Compared with traditional DNNs, the flexibility in uncertainty quantification of DGPs makes them ideal candidate for surrogate modeling (Radaideh and Kozlowski, 2020; Sauer et al., 2022). DGPs are commonly used statistical surrogates in many applications such as Bayesian optimization (Hebbal et al., 2021), calibration (Marmin and Filippone, 2022), multi-fidelity analysis (Ko and Kim, 2021),

healthcare (Li et al., 2021), and etc.

However, training and inference of DGPs are difficult. Current attempts can be separated into two classes. One focuses on designing more efficient and accurate training algorithm while the other one on constructing DGP architectures with sparsity. Efficient training and inference algorithms include expectation propagation (Bui et al., 2016), doubly stochastic variational inference (Salimbeni and Deisenroth, 2017), stochastic gradient Hamiltonian Monte Carlo (Havasi et al., 2018), elliptical slice sampling (Sauer et al., 2022), Vecchia approximation (Vecchia, 1988; Sauer et al., 2022a; Katzfuss and Guinness, 2021), and etc. Reformulation of DGPs to simplified models is an alternative approach. DGPs are reformulated as an variational model in Tran et al. (2016). Low-rank approximations for GPs in Banerjee et al. (2008); Cressie and Johannesson (2008) are also extended to DGPs. Hensman and Lawrence (2014); Dai et al. (2016) extend the inducing-variable method to DGPs. Cutajar et al. (2017) uses random Fourier feature expansion to show that DGPs are equivalent to infinitely wide BNN with corresponding activations.

In this work, we consider DGPs with Markov structure and, based on the Markov structure, we design an accurate and efficient sparse expansion for DGPs. Sidén and Lindsten (2020) proposes compositions of *discrete* Gaussian Markov random field on graph and called deep graphical models of this structure *Deep Gaussian Markov Random Fields* (DGMRF). We must point out that our DTMGPs is essentially different from DGMRF because DTMGPs are *not* deep graphical models. More specifically, DGMRF treats every activation as a random variable and imposes a graphical Markov structure on these activations, i.e., any two non-adjacent randomly distributed activations are conditionally independent given all other activations. On the other hand, every activation in DTMGP is one of the orthonormal basis functions of a *continuous* Gaussian Markov random field and these orthonormal basis functions constitute a so-called *hierarchical expansion* of the field.

## 3 General DGP Models

### 3.1 Deep Gaussian Processes

A GP  $\mathcal{G}$  is a random function characterized by its mean function  $\mu$  and covariance function  $k$ . To be more specific, given any input  $\mathbf{x}$ , the output  $\mathcal{G}(\mathbf{x})$  has a Gaussian distribution

with mean  $\mu(\mathbf{x})$  and variance  $k(\mathbf{x}, \mathbf{x})$ , and given any pair of inputs  $\mathbf{x}$  and  $\mathbf{x}'$ , the covariance between  $\mathcal{G}(\mathbf{x})$  and  $\mathcal{G}(\mathbf{x}')$  is  $k(\mathbf{x}, \mathbf{x}')$ :

$$\begin{aligned}\mathcal{G}(\mathbf{x}) &\sim \mathcal{N}(\mu(\mathbf{x}), k(\mathbf{x}, \mathbf{x})), \\ \mathbf{Cov}(\mathcal{G}(\mathbf{x}), \mathcal{G}(\mathbf{x}')) &= k(\mathbf{x}, \mathbf{x}').\end{aligned}\tag{1}$$

A  $W$ -variate GP is simply a  $W$ -vector of GPs  $[\mathcal{G}_1, \mathcal{G}_2, \dots, \mathcal{G}_W]$ . Without loss of generality, we assume that any multivariate GP in the following content has mean function  $\mu = 0$  and independently distributed entries. A  $H$ -layer DGP  $\mathbf{f}^{(H)}$  is then the composition of  $H$  multi-variate GPs:

$$\mathbf{f}^{(H)}(\mathbf{x}^*) = \mathcal{G}^{(H)} \circ \dots \circ \mathcal{G}^{(2)} \circ \mathcal{G}^{(1)}(\mathbf{x}^*),\tag{2}$$

where  $f \circ g$  denotes the composition function  $f(g(\cdot))$ ,  $\mathcal{G}^{(h)}$  denotes a  $W^{(h)}$ -variate GP  $[\mathcal{G}_1^{(h)}, \mathcal{G}_2^{(h)}, \dots, \mathcal{G}_{W^{(h)}}^{(h)}]$ , and  $W^{(h)}$  is called the width of layer  $h$ . The formulation (2) of DGP can be viewed as a DNN with random activations  $\{\mathcal{G}_i^{(h)}\}$ .

While DGP yields a non-parametric and Bayesian formulation of DNNs, computations for inference/prediction of DGPs are cumbersome. For example, given a set of input-output pairs  $(\mathbf{X}, \mathbf{Y}) \in \mathbb{R}^{n \times d} \times \mathbb{R}^n$ , the conditional probability distribution  $\mathbb{P}(\mathbf{Y}|\mathbf{X})$  induced by (2) is

$$\mathbb{P}(\mathbf{Y}|\mathbf{X}) = \int \mathbb{P}(\mathbf{Y}|\mathbf{f}^{(H)})\mathbb{P}(\mathbf{f}^{(H-1)}|\mathbf{f}^{(H-2)}) \dots \mathbb{P}(\mathbf{f}^{(1)}|\mathbf{X})d\mathbf{f}^{(1)} \dots d\mathbf{f}^{(H)},\tag{3}$$

where  $\mathbf{f}^{(h)}$  denotes the output vector from layer  $h$ :

$$\mathbf{f}^{(h)} = \mathcal{G}^{(h)} \circ \mathcal{G}^{(h-1)} \circ \dots \circ \mathcal{G}^{(1)},$$

with  $h = 1, \dots, H$ . Evidently, the integral (3) is intractable, leading to the intractability of inference and predictions of DGP  $\mathbf{f}^{(H)}$  conditioned on any observed data  $(\mathbf{X}, \mathbf{Y})$ .

## 3.2 Induced Approximation of DGPs

The inference of GP, which acts as a single activation in DGP, is also time and space consuming. A challenge for GPs lies in their computational complexity and storage for the inverse of covariance matrix  $k(\mathbf{X}, \mathbf{X})$  which are  $\mathcal{O}(n^3)$  and  $\mathcal{O}(n^2)$ , respectively, when the covariance matrix is of size  $n$ . To alleviate this computational problem, current methods, such as inducing-variable approximation in Hensman and Lawrence (2014); Dai et al. (2016)

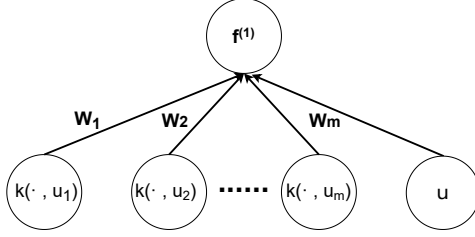


Figure 1: Induced approximation  $\hat{\mathcal{G}}$  can be represented as a one-layer neural network with correlated Gaussian distributed weights  $\mathbf{w} = [k(\mathbf{U}, \mathbf{U})]^{-1}\mathcal{G}(\mathbf{U})$  and bias  $\mu$ .

and random Fourier feature approximation in Cutajar et al. (2017), focus on approximating the covariance matrix  $k(\mathbf{X}, \mathbf{X})$  by some low rank matrices.

Instead of approximating the covariance matrix, we approximate the GP activations in a DGP directly. In the following content, we will construct a reduced-rank approximation called induced approximation. Induced approximation can bring a more flexible and clear deep neural network representation of DGPs.

Without loss of generality, let  $\mathcal{G}$  defined in (1) be a GP with constant mean  $\mu$  and covariance function  $k$ . Inspired by the kriging method (Matheron, 1963; Sacks et al., 1989), we can approximate GP  $\mathcal{G}$  defined in (1) by the following finite-rank approximation:

$$\hat{\mathcal{G}}(\mathbf{x}^*) := \mu + k(\mathbf{x}^*, \mathbf{U})[k(\mathbf{U}, \mathbf{U})]^{-1}\mathcal{G}(\mathbf{U}) \quad (4)$$

where we call  $\mathbf{U} = \{\mathbf{u}_i \in \mathbb{R}^d\}_{i=1}^m$  the inducing points and  $\mathcal{G}(\mathbf{U})$  are the values of  $\mathcal{G}$  on  $\mathbf{U}$ . According to theory in (Ritter, 2000; Wang et al., 2020; Ding and Zhang, 2020), the required number of inducing points for achieving the optimal statistical error is much lower than the sample size, provided that the inducing points  $\mathbf{U}$  are well-chosen. Hence, (4) can be computed in a highly efficient way.

Finite-rank approximation (4) can be represented as a one-layer neural network with correlated Gaussian distributed weights  $\mathbf{w} = [k(\mathbf{U}, \mathbf{U})]^{-1}\mathcal{G}(\mathbf{U})$  and bias  $\mu$  as shown in Figure 1. However, the correlated Gaussian distributed weights still make training and inference difficult. In order to write the finite-rank approximation (4) in the form of a neural network with independently distributed weights, we can simply apply Cholesky decomposition on kernel matrix  $k(\mathbf{U}, \mathbf{U})$ , which leads to the following equation:

$$\hat{\mathcal{G}}(\mathbf{x}^*) = \mu + k(\mathbf{x}^*, \mathbf{U})R_{\mathbf{U}}^{-1}\mathbf{Z} := \mu + \phi^T(\mathbf{x}^*)\mathbf{Z}, \quad (5)$$

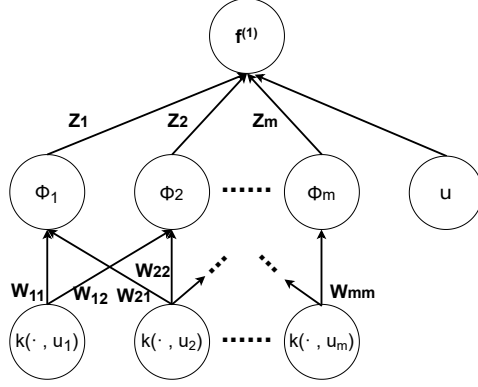


Figure 2: A two-layer neural network representation of  $\hat{\mathcal{G}}$  with deterministic weights  $\mathbf{W} = [R_{\mathbf{U}}^T]^{-1}$ , i.i.d. standard Gaussian weights  $\mathbf{Z}$ , and bias  $\mu$ .

where  $R_{\mathbf{U}}$  is the Cholesky decomposition of matrix  $k(\mathbf{U}, \mathbf{U})$  and  $\mathbf{Z} = [R_{\mathbf{U}}^T]^{-1}\mathcal{G}(\mathbf{U}) \in \mathbb{R}^m$  are i.i.d. distributed standard Gaussian random variables. We call approximation (5) induced approximation and Figure 2 shows that induced approximation can be represented as a two-layer neural network where functions  $\phi$  act as an extra hidden layer. Because the approximation (5) consists of only  $m$  Gaussians, the time and space complexity for its inference are then reduced to  $\mathcal{O}(m^2n)$  and  $\mathcal{O}(mn)$ , respectively.

The induced approximation of a DGP is to approximate each random activation by corresponding induced approximation. For example, suppose that in a DGP  $\mathbf{f}^{(H)}$ , all activations in the same layer are characterized by the same covariance function  $k^{(h)}$ . Then, the induced approximation  $\tilde{\mathbf{f}}^{(H)}$  of  $\mathbf{f}^{(H)}$  is

$$\begin{aligned} \tilde{\mathbf{f}}^{(H)}(\mathbf{x}^*) &= [\mathbf{Z}^{(H)}\phi^{(H)}(\cdot) + \boldsymbol{\mu}^{(H)}] \circ \dots \circ [\mathbf{Z}^{(1)}\phi^{(1)}(\mathbf{x}^*) + \boldsymbol{\mu}^{(1)}], \\ [\phi^{(h)}(\cdot)]^T &= k^{(h)}(\cdot, \mathbf{U}^{(h)})R_h^{-1} \quad \text{for } h = 1, \dots, H \end{aligned} \tag{6}$$

where, for  $h = 1, \dots, H$ ,  $\mathbf{Z}^{(h)} \in \mathbb{R}^{W^{(h)} \times m^{(h)}}$  is a matrix with i.i.d. standard Gaussian entries,  $\mathbf{U}^{(h)}$  are the total  $m^{(h)}$  inducing variables for kernel  $k^{(h)}$ ,  $R_h \in \mathbb{R}^{m^{(h)} \times m^{(h)}}$  is the Cholesky decomposition of the covariance matrix  $k^{(h)}(\mathbf{U}^{(h)}, \mathbf{U}^{(h)})$ , and  $\boldsymbol{\mu}^{(h)} \in \mathbb{R}^{W^{(h)}}$  is the mean vector and can be treated as the bias of layer  $h$ .

In the next section, we will show that if kernel  $k$  is in a class of kernel function called tensor Markov kernel and inducing points  $\mathbf{U}$  are a specific design called sparse grid, then induced approximations (5) and (6) can be further written as a sparse approximation.

## 4 Methodology of DTMGP

In this section, we first introduce the concept of TMGPs. We then introduce hierarchical expansion of TMGPs and how it leads to mutually orthogonal feature functions with hierarchical supports. Based on hierarchical expansion, we can introduce the implementation and training of DTMGPs.

### 4.1 Tensor Markov GPs

Hierarchical expansion is applied to a class of GPs called tensor Markov GP. In one dimension, a Markov GP is characterized by the following Lemma in Marcus and Rosen (2006):

**Lemma 1** (Marcus and Rosen (2006) Lemma 5.1.8). *Let  $I \subseteq \mathbb{R}$ . Let  $\mathcal{G}$  be a zero mean GP defined on  $I$  with continuous positive definite kernel  $k$ . Then,  $\mathcal{G}$  is a Markov GP and  $k$  is Markov kernel if and only if there exist positive functions  $p$  and  $q$  on  $I$  with  $p/q$  strictly increasing such that*

$$k(x, x') = p(\min(x, x'))q(\max(x, x')), \quad x, x' \in I. \quad (7)$$

For any Markov GP  $\mathcal{G}$  we have that, conditioned on its distribution at a point  $x$ , its distributions at any point  $x_l < x$  and any point  $x_u > x$  are independent:  $\mathcal{G}(x_l) \perp \mathcal{G}(x_u) | \mathcal{G}(x)$ , whence Markov GP. Markov GPs have two advantages in computations. Firstly, given any ordered inducing points  $\{u_1 < \dots < u_n\}$ , the distribution of  $\mathcal{G}(x)$  at any  $x$ , where  $u_i < x < u_{i+1}$ , depends only on its left and right inducing points  $\mathcal{G}(u_i)$  and  $\mathcal{G}(u_{i+1})$ . Secondly, for any induced approximation, accuracy of the approximation at  $x$  only depends on the distances between  $x$  and its left and right neighbors, respectively. Therefore, evenly distributed inducing variables can achieve an accurate approximation that is also cheap to compute.

The following purely *additive* and purely *tensor* structure of one-dimensional Markov kernel can both extend Markov GPs to multi-dimension:

$$k(\mathbf{x}, \mathbf{x}') = \sum_{j=1}^d k_j(x_j, x'_j), \quad k(\mathbf{x}, \mathbf{x}') = \prod_{j=1}^d k_j(x_j, x'_j). \quad (8)$$

We generalize the additive and tensor form in (8) to the following GP, which has additive and tensor structure simultaneously:



**Definition 1.** A GP is called TMGP if and only if it is a zero mean GP with covariance function of the form

$$k(\mathbf{x}, \mathbf{x}') = \sum_{l=1}^s \prod_{j \in \mathbf{U}_l} k_{l,j}(x_j, x'_j), \quad (9)$$

where  $\mathbf{U}_l \subseteq \{1, 2, \dots, d\}$  and  $k_{l,j}$  is 1-D Markov kernel for any  $l, j$ . A kernel of the form (10) is called tensor Markov kernel (TMK).

A TMGP  $\mathcal{G}$  with kernel (9) can be factorized as sum of  $s$  mutually independent GPs:  $\mathcal{G} = \sum_{l=1}^s \mathcal{G}_l$  where each  $\mathcal{G}_l$  is with kernel function  $\prod_{j \in \mathbf{U}_l} k_{l,j}(x_j, x'_j)$ . To achieve an accurate approximation of TMGP using the smallest number of inducing variables, we can only focus on TMGP with a purely tensor structure. By combining mutually independent approximations, we can arrive at a solution. Therefore, in the following content, we only study approximation for TMGP with purely tensor structure:

$$k(\mathbf{x}, \mathbf{x}') = \prod_{j=1}^d k_j(x_j, x'_j), \quad (10)$$

and the general TMGP with kernel (9) is a straightforward extension that involves combining approximations of GPs with purely tensor kernels.

Commonly used TMKs with purely tensor structure include Laplace kernel  $k(\mathbf{x}, \mathbf{x}') = \exp(\sum_{j=1}^d \theta_j |x_j - x'_j|)$  and Brownian sheet kernel  $k(\mathbf{x}, \mathbf{x}') = \prod_{j=1}^d (1 + \theta_j \min\{x_j, x'_j\})$ . The challenge in extending the inducing approximation of 1-D Markov GP to multiple dimensions lies in properly defining the "left" and "right" neighbors in a multidimensional space, similar to how it's done on the real line. To address this, we introduce the hierarchical expansion method, which is explained in the following section.

## 4.2 Hierarchical Expansion

To construct the hierarchical expansion, we let inducing variables  $\mathbf{U}$  be an experimental design  $\mathbf{X}_l^{\text{SG}}$  called level- $l$  *Sparse Grid* (SG) (Bungartz and Griebel, 2004; Plumlee, 2014), where level  $l$  determines the number of inducing variables. Furthermore, the SG inducing variables must be sorted in a specific order. Detailed introduction of SGs and the required order are provided in Appendix A, and MATLAB codes for generating SGs satisfying the requirement can be found in the *Sparse Grid Designs* package (Plumlee, 2021). Examples of two-dimensional SGs are shown in Figure 3. From the examples, we can see that the

incremental points from the next level of a SG exhibit a hierarchical structure – higher level SG consists of local SGs of smaller levels.

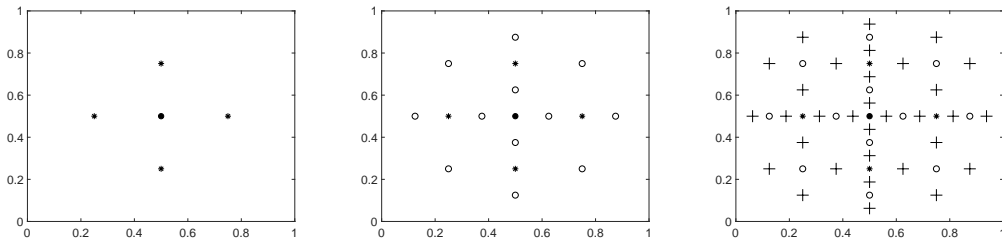


Figure 3: Two-dimensional level-2 SG (left), level-3 SG (middle) and level-4 SG (right) on cube  $(0, 1)^2$ . The incremental points from the second level, third level and fourth level are labeled by \*, o and +, respectively.

Hierarchical expansion of a TMGP  $\mathcal{G}$  with inducing points  $\mathbf{X}_l^{\text{SG}}$  is then simply:

$$\mathcal{G}(\mathbf{x}^*) \approx k(\mathbf{x}^*, \mathbf{X}_l^{\text{SG}})R_l^{-1}\mathbf{Z} := \phi^T(\mathbf{x}^*)\mathbf{Z}, \quad (11)$$

where  $k(\mathbf{x}^*, \mathbf{X}_l^{\text{SG}}) = [k(\mathbf{x}^*, \mathbf{x}_1), \dots, k(\mathbf{x}^*, \mathbf{x}_{m_l})]$  is the covariance vector,  $k(\mathbf{X}_l^{\text{SG}}, \mathbf{X}_l^{\text{SG}}) = [k(\mathbf{x}_i, \mathbf{x}_j)]_{i,j \leq m_l}$  is the covariance matrix,  $R_l$  is the Cholesky decomposition of  $k(\mathbf{X}_l^{\text{SG}}, \mathbf{X}_l^{\text{SG}})$ ,  $\mathbf{Z} = [Z_1, \dots, Z_{m_l}]$  are i.i.d. standard Gaussian random variables and  $\phi = [\phi_i]_{i=1}^{m_l}$  are called hierarchical features. Hierarchical expansion (11) yields a sparse approximation of TMGP that is easy to compute as shown in the following theorems.

**Theorem 1.** *The number of non-zero entries on  $R_l^{-1}$  is  $\mathcal{O}(m_l)$  and  $R_l^{-1}$  can be computed in  $\mathcal{O}(m_l)$  operations.*

**Theorem 2.** *Given any input point  $\mathbf{x}^*$ , the number of non-zero entries on the vector of hierarchical features  $\phi(\mathbf{x}^*)$  is  $\mathcal{O}([\log m_l]^{2d-1})$ .*

The algorithm for computing  $R_l^{-1}$  in  $\mathcal{O}(m_l)$  operations is given in Appendix B, and proofs for Theorems 1 and 2 are provided in supplementary material. Since we can compute  $R_l^{-1}$  in  $\mathcal{O}(m_l)$  operations and the numbers of non-zero entries on  $R_l^{-1}$  is  $\mathcal{O}(m_l)$ , hierarchical expansion can be computed in  $\mathcal{O}(m_l)$  operations. Moreover, if matrix  $R_l^{-1}$  is given, because the numbers of non-zero entries on  $\phi(\mathbf{x}^*)$  is only  $\mathcal{O}([\log m_l]^{2d-1})$ , the computational time of the hierarchical expansion can be further reduced to  $\mathcal{O}([\log m_l]^{2d-1})$ . The sparsity of

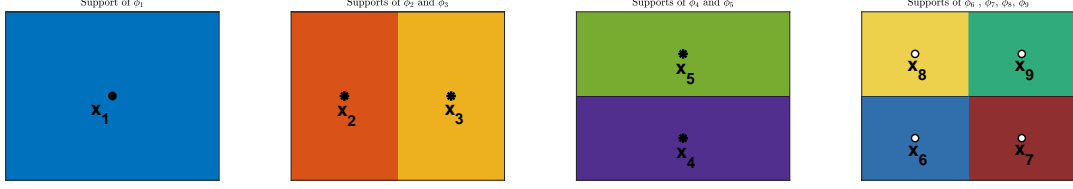


Figure 4: Support of hierarchical feature  $\phi_1$  corresponding to  $\mathbf{x}_1$  in level 1 (left); supports of  $\{\phi_i\}_{i=2}^5$  corresponding to  $\{\mathbf{x}_i\}_{i=2}^5$  (middle figures); supports of  $\{\phi_i\}_{i=6}^9$  corresponding to  $\{\mathbf{x}_i\}_{i=6}^9$  in level 3 (right).

hierarchical feature vector  $\phi$  relies on the fact that the supports of  $\{\phi_i\}_{i=1}^{m_l}$  are either nested or disjoint and, hence, form a hierarchical structure as shown in Figure 4.

$\mathbf{X}_l^{\text{SG}}$  is also regarded as the index set of  $\phi$ , because instead of labeling each hierarchical feature by number  $i$ , we can also label it by the corresponding inducing variable  $\mathbf{x}_i \in \mathbf{X}_l^{\text{SG}}$ . As shown in Figure 5, for any  $i$ ,  $\mathbf{x}_i$  is the only point at which  $\phi_i$  is not differentiable along all dimensions. Hence, we call  $\mathbf{x}_i$  the center of  $\phi_i$ . From this perspective, we can claim that, given any  $\mathbf{x}^*$ , the distribution of the approximation at  $\mathbf{x}^*$  only depends on  $\mathcal{O}([\log m_l]^{2d-1})$  inducing variables. As a result, the hierarchical expansion generalizes the one-dimensional Markov property while still remaining a high accuracy approximate. We discuss the approximation error of hierarchical expansion in supplementary material.

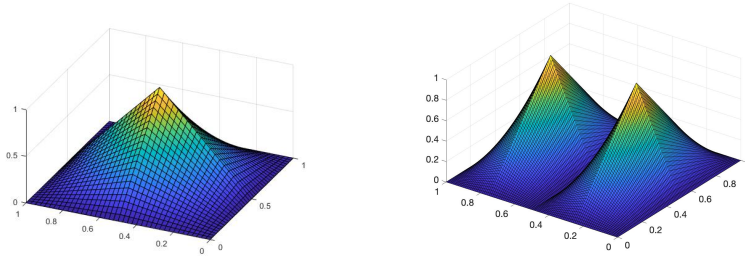


Figure 5: Hierarchical features  $\phi_1$  (left) and  $\phi_2, \phi_3$  (right) generated by the tensor Brownian Bridge kernel  $k(\mathbf{x}, \mathbf{x}') = \prod_{j=1}^2 \min\{x_j, x'_j\}(1 - \max\{x_j, x'_j\})$ .

The following numerical example illustrates the sparsity of hierarchical expansion:

**Example 1.** Let two-dimensional TMK  $k(\mathbf{x}, \mathbf{x}') = \exp\{-\sum_{j=1}^2 |x_j - x'_j|\}$ . Let

$$\mathbf{X}_2^{\text{SG}} = \left[ \left( \frac{1}{2}, \frac{1}{2} \right), \left( \frac{1}{2}, \frac{1}{4} \right), \left( \frac{1}{2}, \frac{3}{4} \right), \left( \frac{1}{4}, \frac{1}{2} \right), \left( \frac{3}{4}, \frac{1}{2} \right) \right],$$

be the sorted level-2 SG. Then, we numerically compute the inverse Cholesky decomposition  $R_2^{-1}$  and we get

$$R_2^{-1} = \begin{bmatrix} 1.0000 & -1.2416 & -1.2416 & -1.2416 & -1.2416 \\ 0 & 1.5942 & 0.0000 & 0.0000 & 0.0000 \\ 0 & 0 & 1.5942 & 0.0000 & 0.0000 \\ 0 & 0 & 0 & 1.5942 & 0.0000 \\ 0 & 0 & 0 & 0 & 1.5942 \end{bmatrix}.$$

Let  $\mathbf{x}_1^* = (0.8147, 0.9058)$ , and  $\mathbf{x}_2^* = (0.2785, 0.5469)$  be two randomly chosen points. We numerically compute the hierarchical features at  $\mathbf{x}_1^*$  and  $\mathbf{x}_2^*$  and we get

$$\begin{aligned} k(\mathbf{x}_1^*, \mathbf{X}_2^{\text{SG}})R_2^{-1} &= [0.4865, 0, 0.3918, 0.0000, 0.3918], \\ k(\mathbf{x}_2^*, \mathbf{X}_2^{\text{SG}})R_2^{-1} &= [0.7646, 0.5291, 0, 0, 0.0933]. \end{aligned}$$

As we can see, matrix  $R_2^{-1}$  is sparse and each of  $k(\mathbf{x}_1^*, \mathbf{X}_2^{\text{SG}})R_2^{-1}$  and  $k(\mathbf{x}_2^*, \mathbf{X}_2^{\text{SG}})R_2^{-1}$  has two zero elements. The sparsity is even more visible as the number of inducing points increases.

### 4.3 Deep Tensor Markov GPs

A  $H$ -layer DTMGP  $\mathcal{T}^{(H)}$  is defined as the composition of  $H$  hierarchical expansions of multi-variate TMGP:

$$\mathcal{T}^{(H)}(\mathbf{x}^*) = [\mathbf{Z}^{(H)}\phi^{(H)}(\cdot) + \boldsymbol{\mu}^{(H)}] \circ \dots \circ [\mathbf{Z}^{(1)}\phi^{(1)}(\mathbf{x}^*) + \boldsymbol{\mu}^{(1)}], \quad (12)$$

where, for  $h = 1, \dots, H$ ,  $\mathbf{Z}^{(h)}$  is a  $W^{(h)}$ -by- $m^{(h)}$  matrix with i.i.d. standard Gaussian entries,  $W^{(h)}$  is the dimension of the output (width of the neural network) of layer  $h$ ,  $m^{(h)}$  is the number of hierarchical features for approximating a  $W^{(h)}$ -variate TMGP,  $\phi^{(h)}$  consists of the  $m^{(h)}$  hierarchical features for approximating the TMGP, acting as the activation functions in layer  $h$ , and  $\boldsymbol{\mu}^{(h)} \in \mathbb{R}^{W^{(h)}}$  is the parameterized mean for the TMGP in layer  $h$ .

Let us now focus on layer  $h$  of  $\mathcal{T}^{(H)}$  to compare DTMGP with DNN. Let  $\mathcal{T}^{(h)} = (\mathcal{T}_1^{(h)}, \dots, \mathcal{T}_{W^{(h)}}^{(h)})$  denote the  $W^{(h)}$ -dimensional output of layer  $h$ . We then have the following structure:

$$\mathcal{T}^{(h-1)} \rightarrow \underbrace{(\phi_1^{(h)}(\mathcal{T}^{(h-1)}), \dots, \phi_{m^{(h)}}^{(h)}(\mathcal{T}^{(h-1)}))}_{\# \text{ non-zero entries: } \mathcal{O}([\log m^{(h)}]2^{W^{(h-1)}-1})} \rightarrow \left[ \mathcal{T}_j^{(h)} = \mu_j^{(h)} + \sum_{i=1}^{m^{(h)}} Z_{j,i} \phi_i^{(h)}(\mathcal{T}^{(h-1)}) \right]_{j=1}^{W^{(h)}},$$

where  $\phi_i^{(h)}(\mathcal{T}^{(h-1)})$  is the  $i^{\text{th}}$  entry of vector  $k^{(h)}(\mathcal{T}^{(h-1)}, \mathbf{X}_{l^{(h)}}^{\text{SG}})[R^{(h)}]^{-1}$ ,  $k^{(h)}$  is the TMK for layer  $h$ ,  $\mathbf{X}_{l^{(h)}}^{\text{SG}}$  is a level- $l^{(h)}$  SG of size  $m^{(h)}$  for induced approximation, and  $R^{(h)}$  is

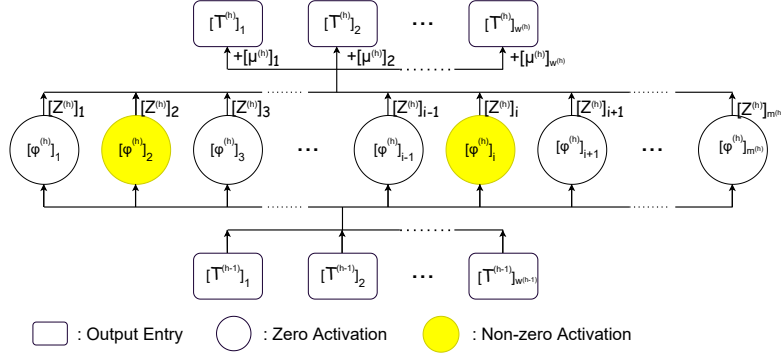


Figure 6: Only  $\mathcal{O}([\log m^{(h)}]2^{W^{(h-1)}}-1)$  activations are non-zero in layer  $h$  of DTMGP  $\mathcal{T}^{(H)}$ .

the Cholesky decomposition of covariance matrix  $k^{(h)}(\mathbf{X}_{l^{(h)}}^{\text{SG}}, \mathbf{X}_{l^{(h)}}^{\text{SG}})$ . This structure is also illustrated in Figure 6.

If we treat DTMGP as a DNN, then, for  $h = 1, \dots, H$ , layer  $h$  is equipped with  $m^{(h)}$  activations  $\{k^{(h)}(\cdot, \mathbf{x}) : \mathbf{x} \in \mathbf{X}_{l^{(h)}}^{\text{SG}}\}$ , a sparse linear filter  $[R^{(h)}]^{-1}$  which converts the dense input to sparse local hierarchical features, bias  $\boldsymbol{\mu}^{(h)}$ , and i.i.d. standard Gaussian weights. Moreover, sparse linear filters  $\{[R^{(h)}]^{-1}\}_{h=1}^H$  are fixed for a specific hierarchical expansion. Therefore,  $\{[R^{(h)}]^{-1}\}_{h=1}^H$  can be computed and stored in advance. Due to Theorems 1 and 2, the space complexity for storing  $\{[R^{(h)}]^{-1}\}_{h=1}^H$  is linear in the number of inducing points and the time complexity of any operation in layer  $h$  of DTMGP is  $\mathcal{O}([\log m^{(h)}]2^{W^{(h-1)}}-1)$ .

## 4.4 Variational Inference

The proposed DTMGP is mathematically equivalent to a deep neural network with biases  $\{\boldsymbol{\mu}^{(h)}\}_{h=1}^H$  and independently and normally distributed weights  $\{\mathbf{Z}^{(h)}\}_{h=1}^H$ . So we can parameterize DTMGP as a BNN with independently and normally distributed weights. Specifically, we regard the variances and means of all Gaussian weights, and the biases as parameters of the BNN. A DTMGP can be represented as a stochastic process  $f_{\boldsymbol{\theta}}$  in the parameterized family  $\mathcal{F}_{\boldsymbol{\theta}}$ :

$$\mathcal{F}_{\boldsymbol{\theta}} = \left\{ \left[ (\boldsymbol{\Sigma}^{(H)} \odot \mathbf{Z}^{(H)} + \mathbf{m}^{(H)})\phi^{(H)} + \boldsymbol{\mu}^{(H)} \right] \circ \dots \circ \left[ (\boldsymbol{\Sigma}^{(1)} \odot \mathbf{Z}^{(1)} + \mathbf{m}^{(1)})\phi^{(1)} + \boldsymbol{\mu}^{(1)} \right] : \right. \\ \left. \left\{ \boldsymbol{\Sigma}^{(h)}, \mathbf{m}^{(h)}, \boldsymbol{\mu}^{(h)} \right\}_{h=1}^H \in \boldsymbol{\Theta} \right\},$$

where  $\Theta$  denotes the set of parameters

$$\Theta := \left\{ \boldsymbol{\Sigma}^{(h)} \in \mathbb{R}_+^{W^{(h)} \times m^{(h)}}, \mathbf{m}^{(h)} \in \mathbb{R}^{W^{(h)} \times m^{(h)}}, \boldsymbol{\mu}^{(h)} \in \mathbb{R}^{W^{(h)}}, h = 1, \dots, H \right\},$$

and  $A \odot B$  denotes the entry-wise multiplication of matrices  $A$  and  $B$ , i.e., the Hadamard product. In other words, the family  $\mathcal{F}_\Theta$  consists of BNNs with activations  $\{\phi^{(h)}\}_{h=1}^H$ , parameterized biases, and normally distributed weights.

Given observations  $(\mathbf{X}, \mathbf{Y})$ , our goal is to search for the parameters  $\boldsymbol{\theta}^*$  that maximizes the marginal likelihood  $\mathbb{P}(\mathbf{Y}|\mathbf{X}, \boldsymbol{\theta})$ . The DTMGP  $f_{\boldsymbol{\theta}^*}$  can best interpret how  $(\mathbf{X}, \mathbf{Y})$  is generated. Computing  $\mathbb{P}(\mathbf{Y}|\mathbf{X}, \boldsymbol{\theta})$  of any DGP involves intractable integral as shown in (3), but we can obtain a tractable lower bound using VI. VI first assigns a prior  $f_{\tilde{\boldsymbol{\theta}}}$  with some  $\tilde{\boldsymbol{\theta}} = \{\tilde{\boldsymbol{\Sigma}}^{(h)}, \tilde{\mathbf{m}}^{(h)}, \tilde{\boldsymbol{\mu}}^{(h)}\}_{h=1}^H$  to the underlying stochastic process generating  $(\mathbf{X}, \mathbf{Y})$  and then maximizes the following *evidence lower bound* (ELBO):

$$\mathcal{E}(\boldsymbol{\theta}) = \mathbb{E}_{f_{\boldsymbol{\theta}}} [\log \Pr(\mathbf{Y}|\mathbf{X}, \boldsymbol{\theta})] - \mathcal{D}_{KL}(f_{\boldsymbol{\theta}} \| f_{\tilde{\boldsymbol{\theta}}}), \quad (13)$$

which is the lower bound of log-likelihood  $\log \Pr(\mathbf{Y}|\mathbf{X}, \boldsymbol{\theta})$ .

In our framework, the term  $\mathbb{E}_{f_{\boldsymbol{\theta}}} [\log \Pr(\mathbf{Y}|\mathbf{X}, \boldsymbol{\theta})]$  is called the *negative energy* and can be explicitly written as

$$\mathbb{E}_{f_{\boldsymbol{\theta}}} [\log \Pr(\mathbf{Y}|\mathbf{X}, \boldsymbol{\theta})] = \mathbb{E}_{\mathbf{Z}^{(1)}, \dots, \mathbf{Z}^{(H)}} [\log \Pr(\mathbf{Y}|\mathbf{X}, \mathbf{Z}^{(1)}, \dots, \mathbf{Z}^{(H)}, \boldsymbol{\theta})].$$

This term now can be efficiently estimated by stochastic optimization based on Monte Carlo methods, such as doubly-stochastic approximation (Hensman and Lawrence, 2014; Dai et al., 2014; Salimbeni and Deisenroth, 2017). The term  $\mathcal{D}_{KL}(f_{\boldsymbol{\theta}} \| f_{\tilde{\boldsymbol{\theta}}})$  is the *KL-divergence* between  $f_{\boldsymbol{\theta}}$  and the prior  $f_{\tilde{\boldsymbol{\theta}}}$  and it can be explicitly written

$$\mathcal{D}_{KL}(f_{\boldsymbol{\theta}} \| f_{\tilde{\boldsymbol{\theta}}}) = \frac{1}{2} \sum_{h=1}^H \sum_{i=1}^{W^{(h)}} \sum_{j=1}^{m^{(h)}} \frac{|[\mathbf{m}^{(h)}]_{i,j} - [\tilde{\mathbf{m}}^{(h)}]_{i,j}|^2}{[\tilde{\boldsymbol{\Sigma}}^{(h)}]_{i,j}^2} + \frac{[\boldsymbol{\Sigma}^{(h)}]_{i,j}^2}{[\tilde{\boldsymbol{\Sigma}}^{(h)}]_{i,j}^2} - 1 - \log \frac{[\boldsymbol{\Sigma}^{(h)}]_{i,j}^2}{[\tilde{\boldsymbol{\Sigma}}^{(h)}]_{i,j}^2}.$$

The computation of  $\mathcal{E}$  is efficient at any  $\boldsymbol{\theta} \in \Theta$ , the training process of DTMGP is simply defined as

$$\boldsymbol{\theta}^* = \arg \max_{\boldsymbol{\theta} \in \Theta} \left\{ \mathbb{E}_{f_{\boldsymbol{\theta}}} [\log \Pr(\mathbf{Y}|\mathbf{X})] - \mathcal{D}_{KL}(f_{\boldsymbol{\theta}} \| f_{\tilde{\boldsymbol{\theta}}}) \right\}. \quad (14)$$

This optimization problem can also be treated as a penalized regression problem where the negative energy term is the model fitness level and the KL-divergence term is the penalty of being far from the DTMGP prior. Equation (14) can be solved efficiently by using the automatic differentiation technique (Neidinger, 2010; Baydin et al., 2018).

## 5 Simulation Studies

In this section, we run simulations on systems with stochastic outputs to access DTMGP’s capacity in modeling stochastic processes. More specifically, in each experiment, output  $Y$  of the underlying system at each input  $\mathbf{x}$  follows an *unknown* distribution  $F(\cdot|\mathbf{x})$ :

$$Y(\mathbf{x}) \sim F(y|\mathbf{x}).$$

A training set  $(\mathbf{X}_{\text{train}}, \mathbf{Y}_{\text{train}})$  is independently collected where  $\mathbf{Y}_{\text{train}} = Y(\mathbf{X}_{\text{train}})$  is the realization of the underlying system on inputs  $\mathbf{X}_{\text{train}}$ . We then train competing models using training set  $(\mathbf{X}_{\text{train}}, \mathbf{Y}_{\text{train}})$ .

Let  $\hat{Y}(\cdot)$  denote a trained model. We first choose a test set  $\mathbf{X}_{\text{test}}$  from the input space. For each input  $\mathbf{x} \in \mathbf{X}_{\text{test}}$ , we sample 100 independent realizations from the true underlying system and from the trained model to get data sets  $\{Y_i(\mathbf{x})\}_{i=1}^{100}$  and  $\{\hat{Y}_i(\mathbf{x})\}_{i=1}^{100}$ , respectively. We then use the two-sample *Kolmogorov–Smirnov* (KS) statistic:

$$D_{\mathbf{x}} = \sup_y \left| \frac{1}{100} \sum_{i=1}^{100} \mathbf{1}_{\{Y_i(\mathbf{x}) \leq y\}} - \frac{1}{100} \sum_{i=1}^{100} \mathbf{1}_{\{\hat{Y}_i(\mathbf{x}) \leq y\}} \right|$$

to quantify the similarity between  $Y$  and  $\hat{Y}$  on input  $\mathbf{x}$ . The smaller  $D_{\mathbf{x}}$  is, the closer the two distributions are. We assess the overall performance of  $\hat{Y}(\cdot)$  via the following averaged two-sample KS statistic over test set  $\mathbf{X}_{\text{test}}$ :

$$D = \frac{1}{|\mathbf{X}_{\text{test}}|} \sum_{\mathbf{x} \in \mathbf{X}_{\text{test}}} D_{\mathbf{x}}.$$

We repeat each experiment  $R$  times and call each a macro-replication from which we obtain  $D_r$ ,  $r = 1, \dots, R$ . Finally, we report the mean and standard deviation

$$\begin{aligned} \bar{D} &= \frac{1}{R} \sum_{r=1}^R D_r, \\ \hat{\sigma} &= \left[ \frac{1}{R} \sum_{r=1}^R (D_r - \bar{D})^2 \right]^{1/2}. \end{aligned}$$

In all experiments, activations of DTMGP are hierarchical features generated from TMGPs with the Laplace covariance function  $k(\mathbf{x}, \mathbf{x}') = \exp\{-\frac{\|\mathbf{x} - \mathbf{x}'\|_1}{d}\}$ . We compare DTMGP with the following existing models:

1. **GP**: standard Gaussian process with squared exponential covariance function.

2. **BNN-ReLU** (Schmidt et al., 1992; Graves, 2011; Blundell et al., 2015): ReLU deep neural networks (Glorot et al., 2011) with parameterized Gaussian distributed weights and biases. VI is used for training BNN-ReLU.
3. **DGP-RFF** (Cutajar et al., 2017): A Random Fourier feature expansion of DGP with each layer represented by Gaussian processes with the Gaussian kernel  $\exp\{-\sum_{j=1}^d w_j |x_j - x'_j|^2\}$ . DGP-RFF is trained with VI approximation provided in Cutajar et al. (2017).
4. **DGP-VEC** (Sauer et al., 2022b) DGP where each activation is GP with Matérn-1/2 kernel. Posterior of the model is approximated through the incorporation of the Vecchia approximation (Katzfuss and Guinness, 2021).

Note that all deep models can be represented by the same architecture and the difference among them lies in their activations. For DTMGP, BNN-ReLU, and DGP-RFF, they are BNN with different deterministic activations and random weights. For DGP-VEC, it is composition of GPs. Therefore, for each data set, we adopt the same architectures for fair comparisons. In other words, except for the specific activations, all deep models are with equal number of layers, widths, weights, and biases.

We conduct experiments with two simulation models: a two-dimensional non-Gaussian random field in Section 5.1, and the expected revenue of a 13-dimensional Stochastic Activity Network problem in Section 5.2. All the experiments are implemented on a computer with macOS, 3.3 GHz Intel Core i5 CPU, and 8 GB of RAM (2133Mhz).

## 5.1 A Non-Gaussian Random Field

In this section, we use the following non-Gaussian and non-stationary random field in two dimensions to assess the sample and computational efficiency of the proposed methodology:

$$Y(\mathbf{x}) = \frac{1}{1 + \exp\{B(\mathbf{x})\}}, \quad \mathbf{x} \in [0, 1]^2$$

where  $B(\mathbf{x})$  is a *Brownian sheet*, which is defined as a zero-mean GP with covariance function  $\prod_{d=1}^2 (1 + \min\{x_d, x'_d\})$ .

In this experiment,  $\mathbf{X}_{\text{train}}$  is randomly collected from  $[0, 1]^2$  and  $\mathbf{Y}_{\text{train}}$  is from independently sample paths of  $B(\mathbf{x})$  on  $\mathbf{X}_{\text{train}}$ . We investigate the performance of each method as the sizes of the training set  $(\mathbf{X}_{\text{train}}, \mathbf{Y}_{\text{train}})$  increase. For each training set, we randomly



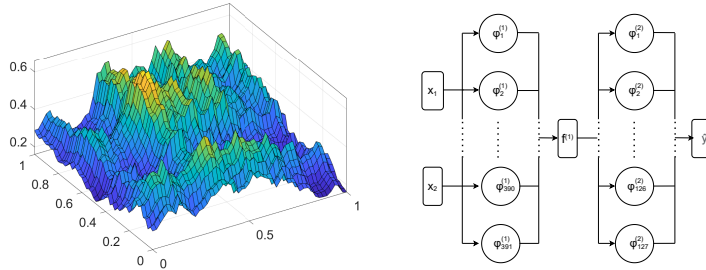


Figure 7: A sample path of non-Gaussian random field  $\frac{1}{1+\exp\{B(\mathbf{x})\}}$ . Right: architecture shared by all deep models to capture the random field.

model	n=40	n=80	n=120	n=160	n=200
DTMGP	28.7 sec	53.5 sec	89.8 sec	138.1 sec	166.4 sec
DGP-VEC	44.2 sec	97.9 sec	255.3 sec	384.2 sec	516.7 sec

Table 1: Time Required to Convergence of Training Error

select  $n_{\text{test}} = 100$  points from  $[0, 1]^2$  as the test set, denoted as  $\mathbf{X}_{\text{test}}$ . We run  $R = 20$  macro-replications and compute  $\hat{D}$  and the associated standard deviation  $\hat{\sigma}$  for each method.

All deep models are with two hidden layers where the first layers consists of 181 activations and 1 output, and the second layer consist of 127 activations and 1 output. Figure 7 shows the realization of the random field and architecture shared by all deep models. We let the i.i.d. prior of each coefficient in DTMGP be normal distributed with mean 0 and variance 1.

Our experiments reveal that DGP-VEC has a significantly longer training time compared to all other models. Specifically, Table 1 demonstrates that while DTMGP has the fastest convergence rate to stable training error, DGP-VEC exhibits the slowest. Consequently, to ensure a fair comparison, we report our results at different training times. First, we report the KS statistics of all models when DTMGP’s training error begins to converge, and then we report the KS statistics of all models when DGP-VEC’s training error begins to converge.

As shown in Figure 7, when given enough training time, DGP-VEC outperforms all other models. However, it’s worth noting that the performance of DTMGP is still comparable to that of DGP-VEC. If we limit the training time for all models to end once the training error of DTMGP begins to converge, we find that DTMGP - which has the fastest convergence

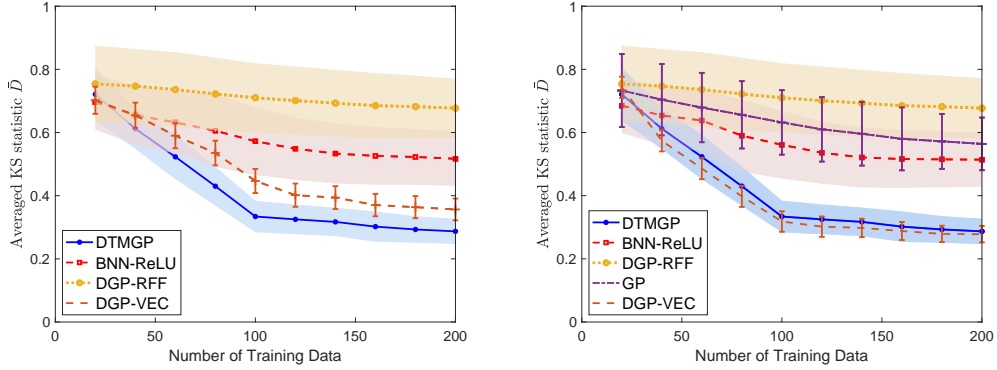


Figure 8: Left:  $\bar{D}$  of each model, the shaded areas and error bars represent 1 std  $\hat{\sigma}$  of all models. Left: results reported when KS statistics of DTMGP begins to converge. Right: results reported when KS statistics of DGP-VEC begins to converge or traing time reaches 4 hours.

rate - outperforms all other models, including DGP-VEC. This is despite the fact that DGP-VEC requires a training time that is three to four times longer than DTMGP, as it relies on MCMC for training. As it is widely acknowledged that VI is more efficient than MCMC, this serves as an important reminder of the tradeoffs we must consider when selecting a training method.

## 5.2 Stochastic Activity Network

In this subsection, we consider the stochastic activity network (SAN) where the arcs are labeled from 1 through 13. The detailed explaiation of SAN is available in Avramidis and Wilson (1996). As shown in the left of Figure 9 , each arc  $i$  in the SAN is associated with a task with random duration  $D_i$  and task durations are mutually independent. Suppose that  $D_i$  is exponentially distributed with mean  $X_i$  for each  $i$ . Suppose that we can control  $X_i > 0$  for each  $i$ , but there is an associated cost. In particular, the overall cost is defined as

$$C(\mathbf{X}) = T(\mathbf{X}) + f(\mathbf{X})$$

where  $\mathbf{X} = (X_1, \dots, X_{13})$ ,  $T(\mathbf{X})$  is the (random) duration of the longest path from a to i, and  $f(\mathbf{X}) = \sum_{i=1}^{13} X_i^{-1}$ . Closed form of  $C(\mathbf{X})$  is unknown but MATLAB simulator of this problem is available in the SimOpt library (Pasupathy and Henderson, 2011).

In this experiment, data are collected from a maximin Latin hypercube design (LHD) that maximizes the minimum distance between points (van Dam et al., 2007). The LHD consists of 5000 sample points from the cube  $[0.5, 5]^{13}$ . At each sample point,  $m$  simulation replications are run with  $m = 2, 4, \dots, 20$ . In order to select reasonable prior for the target stochastic process, we first normalize all the output so that all output data in the training set and testing set are distributed on  $[0, 1]$ . We then run  $m = 10$  replications at each design point during the training process to estimate the variance at each point. Based on the sample estimates, we let the i.i.d. prior of each coefficient in DTMGP be normal distributed with mean 0 and variance 0.04.

We examine the performance of each method as the number of replications  $m$  increase. Given  $m$ , we construct the test set  $\mathbf{X}_{\text{test}}$  of size  $n_{\text{test}} = 100$  by random samples from  $[0.5, 5]^{13}$ . We compute  $\hat{D}$  of each method, its associated standard deviation  $\hat{\sigma}$  based on  $R = 20$  macro-replications.

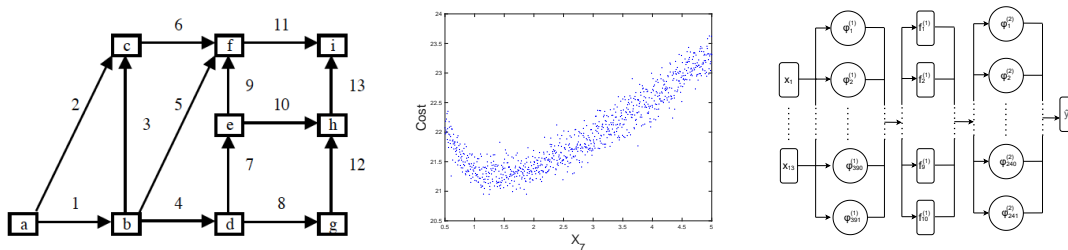


Figure 9: Left: structure of SAN. Middle: i.i.d. samples of  $C(\mathbf{X})$  with  $X_i = 2.5$ ,  $i \neq 7$  and  $X_7 \in [0.5, 5]$ . Right: architecture shared by all competing deep GPs to capture  $C(\mathbf{X})$ .

Similar to section 5.1, all the competing models in this experiment share the same architecture. All deep models have two hidden layers. The first layer consists of 391 activations and its output is 10-dimensional. The second layer consists of 241 activations and its output is 1-dimensional. Such an architecture is flexible enough to capture the random process.

As before, the training time of DGP-VEC is much longer than other models. When  $m > 10$ , the training time required for DGP-VEC is longer than 4 hours, which is unacceptable compared with DTMGP. Therefore, to ensure a fair comparison, we also report our results at different training times. First, we report the KS statistics of all models when DTMGP’s training error begins to converge, and then we report the KS statistics of all models when

model	m=4	m=8	m=12	m=16	m=20
DTMGP	9.5 min	17.8 min	24.3 min	36.7 min	46.2 min
DGP-VEC	1.8 hr	3.2 hr	> 4 hr	> 4 hr	> 4 hr

Table 2: Time Required to Convergence of Training Error

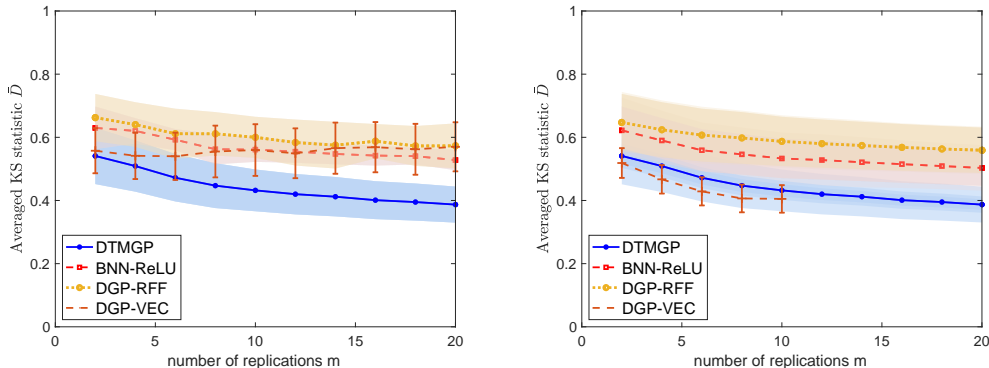


Figure 10:  $\bar{D}$  of each model, the shaded areas and error bars represent 1 std  $\hat{\sigma}$  of all models. Left: results reported when KS statistics of DTMGP begins to converge. Right: results reported when KS statistics of DGP-VEC begins to converge.

DGP-VEC’s training error begins to converge or the training time reaches 4 hours.

As demonstrated in Figure 10, DGP-VEC outperforms all other models when given sufficient training time. However, DGP-VEC’s training time exceeds 4 hours when  $m > 10$  or when the total training data size is greater than 50000. Therefore, we only present the results of DGP-VEC for  $m \leq 10$ . On the other hand, DTMGP demonstrates comparable performance, with a training time of roughly one-tenth that required by DGP-VEC. Similarly to Section 5.1, when we restrict the training time for all models to stop once the training error of DTMGP starts to stabilize, we observe that DTMGP outperforms all other models, and DGP-VEC performs even worse than BNN-ReLU. This is because the training time is not sufficient for MCMC.

## 6 Experiment on Real Data

This section aims to evaluate the performance of the proposed methodology on a real dataset. To this end, we utilize the *RC-49* dataset (Ding et al., 2021), which is a synthetic collection

of 49 3-D chair models rendered at yaw angles ranging from  $0^\circ$  to  $90^\circ$ . The RC-49 dataset consists of  $n = 176400$  data pairs  $(\mathbf{X}, \mathbf{Y}) = \{(x_i, \mathbf{y}_i)\}_{i=1}^n$  where, for any  $i = 1, \dots, n$ , input  $x_i \in [0, 90)$  is a specific yaw angles and outputs  $\mathbf{y}_i$  is a  $64 \times 64$  image of a chair rendered. The objective is to use the Bayesian formula to train a generative model, which is conditioned on the input variable  $x$ . When provided with input yaw angle  $x$ , the trained model should generate a random matrix output that is similar to the data  $\mathbf{Y}$  at the same angle. In essence, the generative problem is a stochastic process  $Y(x) \in \mathbb{R}^{64 \times 64}$  where  $x \in [0, 90)$ , and our aim is to employ a deep GP model to reconstruct  $Y(\cdot)$  from observed data.

We compare DTMGP with BNN-ReLU and DGP-RFF introduced in Section 5. Other deep GP models are omitted due to their limited capacity for handling the large data size and complex model architecture. All competing deep GP models share the following architecture. We first apply the embedding technique on input  $x$ , which uses a linear transformation  $A$  to map the single variable input  $x \in [0, 90)$  to a 100-dimensional vector  $\mathbf{x}' \in \mathbb{R}^{100}$ . We then adopt a four-layer BNN architecture where  $\mathbf{x}'$  is the input layer, the first hidden layer consists of 201 activations and a 256-dimensional output, the second hidden layer consists of 513 activations and a 512-dimensional output, and the third hidden layer consists of 1025 activations and the final output is a  $64 \times 64$  random matrix. Specifically, the architecture can be written as follows:

$$\begin{aligned} f_j^{(1)} &= \sum_{i=1}^{201} Z_{i,j}^{(1)} \phi_i^{(1)}(A\mathbf{x}), \quad j = 1, \dots, 256, \quad Z_{i,j}^{(1)} \sim \mathcal{N}(0, 1), \quad A \in \mathbb{R}^{100 \times 1}, \\ f_j^{(2)} &= \sum_{i=1}^{513} Z_{i,j}^{(2)} \phi_i^{(2)}(f_1^{(1)}, \dots, f_{256}^{(1)}), \quad j = 1, \dots, 512, \quad Z_{i,j}^{(2)} \sim \mathcal{N}(0, 1), \\ \hat{Y}_{l,j} &= \sum_{i=1}^{1025} Z_{i,l,j}^{(3)} \phi_i^{(3)}(f_1^{(2)}, \dots, f_{512}^{(2)}), \quad l, j = 1, \dots, 28, \quad Z_{i,l,j}^{(3)} \sim \mathcal{N}(0, 1). \end{aligned}$$

Figure 11 provides an illustration of the above architecture.

We use 80000 samples from the RC-49 dataset to train DTMGP and its competitors BNN-RELU and DGP-RFF. We train the models by mini-batch SGD and, in each epoch, we sample their random outputs at input  $x$ , for  $x \in [0, 90)$ . Because the output in this experiment is a  $64 \times 64$  random matrix and we are unable to sample data from the true distribution of RC-49, the previous KS statistics cannot be used to access the accuracy. Instead, we directly examine the output images of each model to evaluate their performances.

Conditional samples generated by DTMGP, BNN-ReLU, and DGP-RFF at the 3<sup>rd</sup>, 6<sup>th</sup>

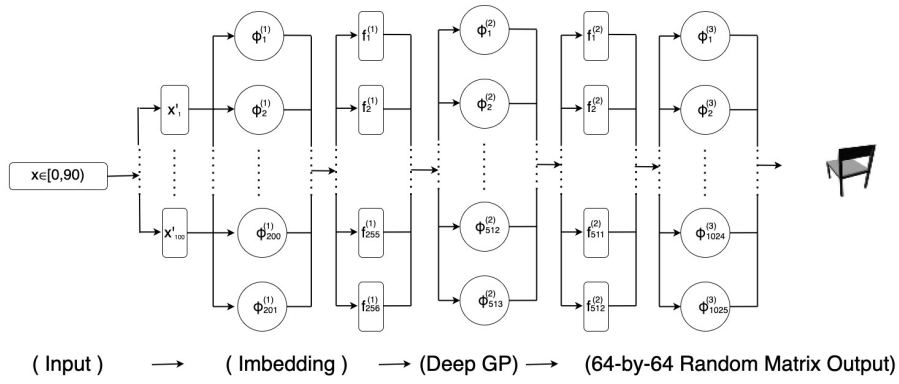


Figure 11: All competing deep GPs share the same architecture.

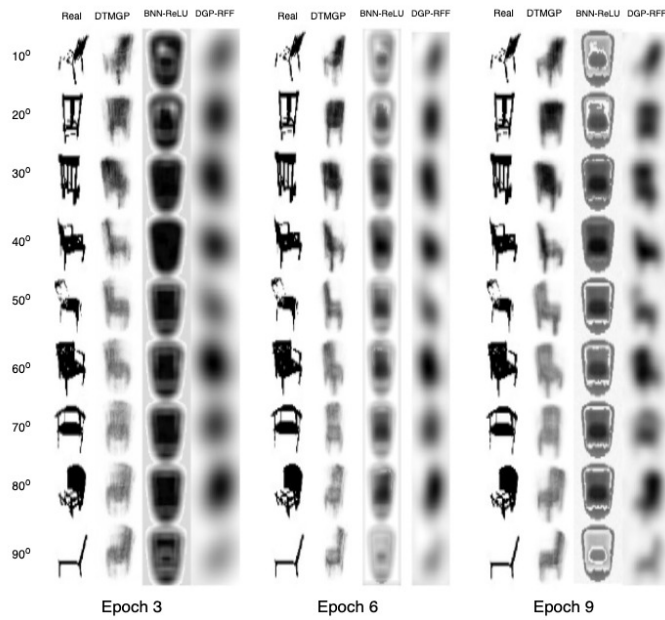


Figure 12: Results at the three epoch (left), six epoch (middle), and nine epoch (right) during training with input  $x = 10, 20, \dots, 90$ .

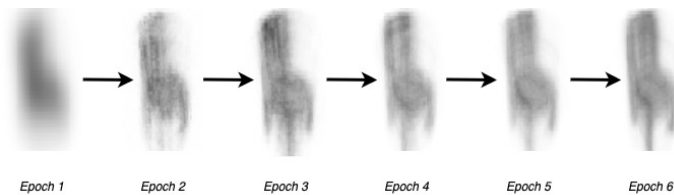


Figure 13: Generated images of DTMGP with  $x=60$

Model	1 Epoch	3 Epoch	6 Epoch	9 Epoch
DTMGP	1099.3 sec	3115.2 sec	6117.6 sec	8953.1 sec
BNN-ReLU	971.5 sec	2511.9 sec	4997.2 sec	7301.1 sec
DGP-RFF	1081.4 sec	2987.7 sec sec	5823.4 sec	8682.8 sec

Table 3: Training Time

and 9<sup>th</sup> epochs are shown in Figure 12. The results demonstrate that DTMGP generates samples that are closer to the actual data and performs the best, while other models fail to reconstruct the conditional samples. This is because, as observed in previous experiments, the hierarchical structure of DTMGP can effectively capture the local features while the ReLU or cosine activations of BNN-ReLU or DGP-RFF lack the ability to do so.

As depicted in Figure 13, DTMGP exhibits a faster convergence rate towards stability with more consistent generated results. The rapid convergence suggests that the model can be trained in few epochs, while the consistent performance implies that the model is reliable. This may be attributed to the sparsity introduced by our expansion approach, which facilitates feature detection and speeds up parameter determination.

Table 3 demonstrates that the training time per epoch of both BNN-ReLU and DGP-RFF is faster than that of DTMGP. This difference could be primarily attributed to the fact that BNN-ReLU and DGP-RFF are built using built-in functions and packages in the MATLAB, while our code for DTMGP does not take this advantage. Nonetheless, the training time per epoch of DTMGP is still comparable to that of BNN-ReLU and DGP-RFF.

## 7 Conclusions and Discussion

We utilize hierarchical features to expand DGPs, which comprise TMGPs. Our expansion is known as DTMGP and is computationally efficient, resulting in a sparse representation of DGPs. The hierarchical nature of the features means that their supports are either nested or disjoint, enabling a poly-logarithmic number of activations throughout a DTMGP to have non-zero output conditioned on any input or operation. Furthermore, hierarchical features can effectively capture local features from inputs, resulting in high performance in prediction and generative problems, as demonstrated in our experiments. In comparison

to existing DGP models, DTMGP’s sparsity leads to efficient inference and training, while generated instances from DTMGP are also relatively accurate under the KS test.

The current paper can potentially be extended in several ways. Firstly, how to apply hierarchical expansion on DGPs with more general structures, such as DGPs with Matérn covariance functions, can be studied in future research. Secondly, it was pointed out by Stein (2014) that, approximating the likelihood function of GP by low-rank methods, such as inducing point and random features, may have an adverse effect on the performance. How large this effect is for the proposed DGP models should be studied in further investigation.

## Acknowledgements

The authors are grateful to the editors and referees for very helpful comments.

## Funding

Tuo’s research is supported by NSF DMS-1914636 and CCF-1934904 and 2022 Texas A&M Institute of Data Science Career Initiation Fellow Program. Part of Ding’s work was conducted when he was a postdoctoral researcher at Texas A&M University and was partially supported by the Texas A&M Institute of Data Science (TAMIDS) Postdoctoral Fellowships.

# Appendix

## A Sparse Grid Designs with Required Order

The class of SG adopted in this work is called *Hyperbolic-cross* SG, which is the union of full grids (FG) with dyadic structures. Without loss of generality, we can assume that all design points are collected from the hypercube  $(0, 1)^d$ , and we start constructing SGs satisfying the required order with the one-dimensional case, which is also called dyadic point set.

A one-dimensional level- $l$  dyadic point set  $\mathbf{X}_l$  with increasing order is simply defined as  $\mathbf{X}_l = \{2^{-l}, 2 \cdot 2^{-l}, \dots, 1 - 2^{-l}\}$ . However, this order cannot result in a sparse representation



of hierarchical expansion. We need to sort the points according to their levels. Firstly, given a level  $l \in \mathbb{N}$ , we define the following set consisting only of odd numbers:

$$\boldsymbol{\rho}(l) = \{1, 3, 5, \dots, 2^l - 1\}.$$

Then given a level- $l$  dyadic point set  $\mathbf{X}_l$  and a level- $(l-1)$  dyadic point set  $\mathbf{X}_{l-1}$ , we can define the sorted incremental set

$$\mathbf{D}_l = \mathbf{X}_l - \mathbf{X}_{l-1} = \{i2^{-l} : i \in \boldsymbol{\rho}(l)\},$$

with  $\mathbf{D}_0 = \emptyset$ . It is straightforward to check that

$$\mathbf{X}_l = \bigcup_{\ell=1}^l \mathbf{D}_\ell, \quad \mathbf{D}_l \cap \mathbf{D}_k = \emptyset, \text{ if } l \neq k.$$

For any incremental set  $\mathbf{D}_l$ , we can label any point in  $\mathbf{D}_l$  by  $x_{l,i}$ ,  $i \in \boldsymbol{\rho}(l)$  so that the label is unique for any point:  $x_{l,i} \neq x_{l',i'}$  if and only if  $(l,i) \neq (l',i')$ . Now we can define the following dyadic set with the required order:

$$\mathbf{X}_l^* = [\mathbf{D}_1, \mathbf{D}_2, \dots, \mathbf{D}_l] = [x_{\ell,i} : \ell \leq l, i \in \boldsymbol{\rho}(\ell)].$$

For example,  $\mathbf{X}_3^* = [\frac{1}{2}, \frac{1}{4}, \frac{3}{4}, \frac{1}{8}, \frac{3}{8}, \frac{5}{8}, \frac{7}{8}]$  with  $\mathbf{D}_1 = [\frac{1}{2}]$ ,  $\mathbf{D}_2 = [\frac{1}{4}, \frac{3}{4}]$ , and  $\mathbf{D}_3 = [\frac{1}{8}, \frac{3}{8}, \frac{5}{8}, \frac{7}{8}]$ , respectively.

We also define the Cartesian product of one-dimensional sorted  $\mathbf{X}_l^*$ 's for later use in Algorithms and proofs. We call this sorted Cartesian product full grid (FG)  $\mathbf{X}_\mathbf{l}^*$  labeled by  $\mathbf{l} = (l_1, \dots, l_d) \in \mathbb{N}^d$ :

$$\mathbf{X}_\mathbf{l}^* = \times_{j=1}^d \mathbf{X}_{l_j}^* = [(x_{l_1, i_1}, x_{l_2, i_2}, \dots, x_{l_d, i_d}) : \ell_j \leq l_j, i_j \in \boldsymbol{\rho}(\ell_j), j = 1, \dots, d].$$

For simplicity, we define the Cartesian product  $\boldsymbol{\rho}(\mathbf{l}) = \times_{j=1}^d \boldsymbol{\rho}(l_j)$  for any  $\mathbf{l} \in \mathbb{N}^d$  so that any points in  $\mathbf{X}_\mathbf{l}^*$  can be represented as  $\mathbf{x}_{\mathbf{l}, \mathbf{i}} = (x_{l_1, i_1}, x_{l_2, i_2}, \dots, x_{l_d, i_d})$  for any  $\mathbf{l} \in \mathbb{N}^d$  and  $\mathbf{i} \in \boldsymbol{\rho}(\mathbf{l})$ . Then we have a more compact representation of  $\mathbf{X}_\mathbf{l}^*$ :

$$\mathbf{X}_\mathbf{l}^* = [\mathbf{x}_{\ell, \mathbf{i}} : \ell \leq \mathbf{l}, \mathbf{i} \in \boldsymbol{\rho}(\ell)].$$

For example, the sorted FG  $\mathbf{X}_{(1,2)}^*$  is

$$\mathbf{X}_{(1,2)}^* = [(\frac{1}{2}, \frac{1}{2}), (\frac{1}{2}, \frac{1}{4}), (\frac{1}{2}, \frac{3}{4})].$$

Finally, a level- $l$  SG satisfying our required order is the union of sorted FGs as follows:

$$\mathbf{X}_l^{\text{SG}} = \bigcup_{|\mathbf{l}|=l+d-1} \mathbf{X}_{\mathbf{l}}^* = [\mathbf{x}_{\mathbf{l},\mathbf{i}} : |\mathbf{l}| \leq l, \mathbf{i} \in \boldsymbol{\rho}(\mathbf{l})],$$

where  $|\mathbf{l}|$  denote the  $l_1$  norm  $\sum_{j=1}^d |l_j|$ . To be more specific, a point  $\mathbf{x}_{\mathbf{l},\mathbf{i}} \in \mathbf{X}_l^{\text{SG}}$  must be ahead of any  $\mathbf{x}_{\mathbf{l}'}$  with  $|\mathbf{l}'| > |\mathbf{l}|$ . For example, the two-dimensional sorted SG  $\mathbf{X}_2^{\text{SG}}$  is

$$\mathbf{X}_2^{\text{SG}} = [ \underbrace{\left(\frac{1}{2}, \frac{1}{2}\right)}_{\text{level } |(1,1)|=2}, \underbrace{\left(\frac{1}{2}, \frac{1}{4}\right), \left(\frac{1}{2}, \frac{3}{4}\right)}_{\text{level } |(1,2)|=3}, \underbrace{\left(\frac{1}{4}, \frac{1}{2}\right), \left(\frac{3}{4}, \frac{1}{2}\right)}_{\text{level } |(2,1)|=3} ].$$

Unlike FG, whose size increases exponentially in dimension  $d$ , the size of SGs increases relatively mildly in  $d$ . Lemma 3.6 in Bungartz and Griebel (2004) stipulates that the sample size of a  $d$ -dimensional level- $l$   $\mathbf{X}_l^{\text{SG}}$  is given by

$$|\mathbf{X}_l^{\text{SG}}| = \sum_{\ell=0}^{l-1} 2^\ell \binom{\ell+d-1}{d-1} = 2^l \cdot \left( \frac{l^{d-1}}{(d-1)!} + \mathcal{O}(l^{d-2}) \right) = \mathcal{O}(2^l l^{d-1}). \quad (15)$$

## B Algorithms

We first introduce how to compute  $R^{-1}$ , with  $R$  the Cholesky decomposition of  $k(\mathbf{X}_l^*, \mathbf{X}_l^*)$ ,  $k$  is a one-dimensional Markov kernel and  $\mathbf{X}_l^*$  is a one-dimensional sorted level- $l$  dyadic point set. To present the algorithm for computing the inverse of Cholesky decomposition, we also label the entries on matrices by points in  $\mathbf{X}_l^*$ . For example,  $[R^{-1}]_{x,x'}$  represents entry with row index corresponding to point  $x \in \mathbf{X}_l^*$  and column index corresponding to point  $x' \in \mathbf{X}_l^*$ .

Now let  $k = \prod_{j=1}^d k_j$  be a  $d$ -dimensional TMK and  $\mathbf{X}_1^* = \times_{j=1}^d \mathbf{X}_{l_j}^*$  be a sorted FG. Then,  $R_1^{-1}$ , with  $R_1$  the Cholesky decomposition of  $k(\mathbf{X}_1^*, \mathbf{X}_1^*)$  can be directly calculated as

$$R_1^{-1} = \bigotimes_{j=1}^d R_{l_j}^{-1}, \quad (17)$$

where  $\bigotimes$  denotes the Kronecker product between matrices and  $R_{l_j}^{-1}$  is the inverse Cholesky decomposition yielded by Algorithm 1 with input  $k_j$  and  $\mathbf{X}_{l_j}^*$ .

Let  $R_{\mathbf{X}_1^*, \mathbf{X}_1^*}$  represent a sub-matrix of  $R$  consisting of entries  $R_{\mathbf{x}, \mathbf{y}}$ ,  $\mathbf{x}, \mathbf{y} \in \mathbf{X}_1^* \subset \mathbf{X}_l^{\text{SG}}$ . Now we can present the algorithm of constructing  $R_l^{-1}$

We will prove the correctness of Algorithm 1 and Algorithm 2 in the supplementary material.

---

**Algorithm 1:** Computing  $R^{-1}$  for Markov kernel  $k$  and point set  $\mathbf{X}_l^*$

---

**Input** : Markov kernel  $k$ , level- $l$  dyadic points  $\mathbf{X}_l^*$

**Output** :  $R^{-1}$

```

1 Initialize  $R^{-1} \leftarrow \mathbf{0} \in \mathbb{R}^{(2^l-1) \times (2^l-1)}$ ,  $\mathbf{N} = \{-\infty, \infty\}$ , define  $k(\pm\infty, x) = 0, \forall x$ 
2 for  $\ell \leftarrow 1$  to  $l$  do
3   for  $i \in \rho(\ell)$  do
4     search the closest left neighbor  $x_{left}$  and right neighbor  $x_{right}$  of  $x_{\ell,i}$  in  $\mathbf{N}$ 
5     Solve  $c_1, c_2$ , and  $c_3$  for the following system:
        
$$c_1k(x_{left}, x_{left}) + c_2k(x_{\ell,i}, x_{left}) + c_3k(x_{right}, x_{left}) = 0,$$

        
$$c_1k(x_{left}, x_{right}) + c_2k(x_{\ell,i}, x_{right}) + c_3k(x_{right}, x_{right}) = 0, \quad (16)$$

        
$$\mathbb{E}[(c_1\mathcal{G}(x_{left}) + c_2\mathcal{G}(x_{\ell,i}) + c_3\mathcal{G}(x_{right}))^2] = 1$$

6     If  $x_{left} \neq -\infty$ ,  $[R^{-1}]_{x_{left}, x_{\ell,i}} = c_1$ 
7     If  $x_{right} \neq \infty$ ,  $[R^{-1}]_{x_{right}, x_{\ell,i}} = c_3$ 
8     Let  $[R^{-1}]_{x_{\ell,i}, x_{\ell,i}} = c_2$ ,  $x_{\ell,i} \rightarrow \mathbf{N}$ 
9   end
10 end
11 Return  $R^{-1}$ 

```

---

## References

- Ankenman, B., B. L. Nelson, and J. Staum (2010). Stochastic kriging for simulation metamodeling. *Oper. Res.* 58(2), 371–382.
- Avramidis, A. N. and J. R. Wilson (1996). Integrated variance reduction strategies for simulation. *Operations Research* 44(2), 327–346.
- Banerjee, S., A. E. Gelfand, A. O. Finley, and H. Sang (2008). Gaussian predictive process models for large spatial data sets. *Journal of the Royal Statistical Society: Series B (Statistical Methodology)* 70(4), 825–848.
- Baydin, A. G., B. A. Pearlmutter, A. A. Radul, and J. M. Siskind (2018). Automatic differentiation in machine learning: A survey. *Journal of Machine Learning Research* 18(153), 1–43.
- Blei, D. M., A. Kucukelbir, and J. D. McAuliffe (2017, Apr). Variational inference: A review for statisticians. *Journal of the American Statistical Association* 112(518), 859–877.
- Blundell, C., J. Cornebise, K. Kavukcuoglu, and D. Wierstra (2015). Weight uncertainty

---

**Algorithm 2:** Computing  $R_l^{-1}$  for TMK  $k$  and level- $l$  SG  $\mathbf{X}_l^{\text{SG}}$

---

**Input** : TMK  $k$ , level- $l$  SG  $\mathbf{X}_l^{\text{SG}}$

**Output** :  $R_l^{-1}$

- 1 Initialize  $R^{-1} \leftarrow \mathbf{0} \in \mathbb{R}^{m_l \times m_l}$
- 2 **for** all  $\mathbf{l} \in \mathbb{N}^d$  with  $l \leq |\mathbf{l}| \leq l + d - 1$  **do**
- 3     Compute  $R_{\mathbf{l}}^{-1}$  associated to  $(k, \mathbf{X}_{\mathbf{l}}^*)$  via Algorithm 1 and (17)
- 4     Update  $R_l^{-1}$  via
 
$$[R_l^{-1}]_{\mathbf{x}_1^*, \mathbf{x}_1^*} \leftarrow [R_{\mathbf{l}}^{-1}]_{\mathbf{x}_1^*, \mathbf{x}_1^*} + (-1)^{l+d-1-|\mathbf{l}|} \binom{d-1}{l+d-1-|\mathbf{l}|} R_{\mathbf{l}}^{-1} \quad (18)$$
- 5 **end**
- 6 Return  $R_l^{-1}$

---

in neural network. In *International Conference on Machine Learning*, pp. 1613–1622. PMLR.

Bui, T., D. Hernandez-Lobato, J. Hernandez-Lobato, Y. Li, and R. Turner (2016, 20–22 Jun). Deep Gaussian processes for regression using approximate expectation propagation. Volume 48 of *Proceedings of Machine Learning Research*, New York, New York, USA, pp. 1472–1481. PMLR.

Bungartz, H.-J. and M. Griebel (2004). Sparse grids. *Acta Numerica* 13, 147–269.

Cressie, N. and G. Johannesson (2008). Fixed rank kriging for very large spatial data sets. *Journal of the Royal Statistical Society: Series B (Statistical Methodology)* 70(1), 209–226.

Cutajar, K., E. V. Bonilla, P. Michiardi, and M. Filippone (2017, 06–11 Aug). Random feature expansions for deep Gaussian processes. Volume 70 of *Proceedings of Machine Learning Research*, International Convention Centre, Sydney, Australia, pp. 884–893. PMLR.

Dai, B., B. Xie, N. He, Y. Liang, A. Raj, M.-F. F. Balcan, and L. Song (2014). Scalable kernel methods via doubly stochastic gradients. In Z. Ghahramani, M. Welling, C. Cortes, N. D. Lawrence, and K. Q. Weinberger (Eds.), *Advances in Neural Information Processing Systems* 27, pp. 3041–3049. Curran Associates, Inc.

Dai, Z., A. Damianou, J. González, and N. Lawrence (2016). Variational auto-encoded deep Gaussian processes. *Proceedings of the International Conference on Learning Representations (ICLR) 2016*.

Damianou, A. and N. Lawrence (2013). Deep Gaussian processes. Volume 31 of *Proceedings of Machine Learning Research*, Scottsdale, Arizona, USA, pp. 207–215. PMLR.

- Ding, L. and X. Zhang (2020). Sample and computationally efficient simulation metamodeling in high dimensions. *arXiv preprint arXiv:2010.06802*.
- Ding, X., Y. Wang, Z. Xu, W. J. Welch, and Z. J. Wang (2021). Cegan: Continuous conditional generative adversarial networks for image generation. In *International conference on learning representations*.
- Fei, J., J. Zhao, S. Sun, and Y. Liu (2018). Active learning methods with deep Gaussian processes. In *International Conference on Neural Information Processing*, pp. 473–483. Springer.
- Glorot, X., A. Bordes, and Y. Bengio (2011, 11–13 Apr). Deep sparse rectifier neural networks. Volume 15 of *Proceedings of Machine Learning Research*, Fort Lauderdale, FL, USA, pp. 315–323. JMLR Workshop and Conference Proceedings.
- Graves, A. (2011). Practical variational inference for neural networks. In J. Shawe-Taylor, R. S. Zemel, P. L. Bartlett, F. Pereira, and K. Q. Weinberger (Eds.), *Advances in Neural Information Processing Systems 24*, pp. 2348–2356. Curran Associates, Inc.
- Havasi, M., J. M. Hernández-Lobato, and J. J. Murillo-Fuentes (2018). Inference in deep Gaussian processes using Stochastic Gradient Hamiltonian Monte Carlo. In S. Bengio, H. Wallach, H. Larochelle, K. Grauman, N. Cesa-Bianchi, and R. Garnett (Eds.), *Advances in Neural Information Processing Systems*, Volume 31. Curran Associates, Inc.
- Hebbal, A., L. Brevault, M. Balesdent, E.-G. Talbi, and N. Melab (2021). Bayesian optimization using deep Gaussian processes with applications to aerospace system design. *Optimization and Engineering* 22(1), 321–361.
- Hensman, J. and N. D. Lawrence (2014). Nested variational compression in deep Gaussian processes.
- Hinton, G. (2010). A practical guide to training restricted Boltzmann machines (version 1). *Technical Report UTML TR 2010-003, University of Toronto* 9.
- Hinton, G., S. Osindero, and Y.-W. Teh (2006, 08). A fast learning algorithm for deep belief nets. *Neural Computation* 18, 1527–54.
- Katzfuss, M. and J. Guinness (2021). A general framework for vecchia approximations of gaussian processes. *Statistical Science* 36(1), 124–141.
- Ko, J. and H. Kim (2021). Deep Gaussian process models for integrating multifidelity experiments with non-stationary relationships. *IISE Transactions* (just-accepted), 1–28.
- Li, Y., S. Rao, A. Hassaine, R. Ramakrishnan, D. Canoy, G. Salimi-Khorshidi, M. Mamouei, T. Lukasiewicz, and K. Rahimi (2021). Deep Bayesian Gaussian processes for uncertainty estimation in electronic health records. *Scientific Reports* 11(1), 1–13.
- MacKay, D. J. (1992). A practical Bayesian framework for backpropagation networks. *Neural Computation* 4(3), 448–472.
- Marcus, M. B. and J. Rosen (2006). *Markov Processes, Gaussian Processes, and Local Times*. Cambridge University Press.

- Marmin, S. and M. Filippone (2022). Deep gaussian processes for calibration of computer models. *Bayesian Analysis* 1(1), 1–30.
- Matheron, G. (1963). Principles of geostatistics. *Econ. Geol.* 58(8), 1246–1266.
- Neal, R. M. (1996). *Bayesian learning for neural networks*, Volume 118. Springer Science & Business Media.
- Neidinger, R. D. (2010). Introduction to automatic differentiation and matlab object-oriented programming. *SIAM review* 52(3), 545–563.
- Pasupathy, R. and S. G. Henderson (2011). Simopt: A library of simulation optimization problems. In *Proceedings of the 2011 Winter Simulation Conference (WSC)*, pp. 4075–4085.
- Plumlee, M. (2014). Fast prediction of deterministic functions using sparse grid experimental designs. *J. Amer. Statist. Assoc.* 109(508), 1581–1591.
- Plumlee, M. (2021). Sparse grid designs. <https://www.mathworks.com/matlabcentral/fileexchange/45668-sparse-grid-designs>. MATLAB Central File Exchange.
- Plumlee, M. and R. Tuo (2014). Building accurate emulators for stochastic simulations via quantile kriging. *Technometrics* 56(4), 466–473.
- Radaideh, M. I. and T. Kozlowski (2020). Surrogate modeling of advanced computer simulations using deep Gaussian processes. *Reliability Engineering & System Safety* 195, 106731.
- Rahimi, A. and B. Recht (2008). Random features for large-scale kernel machines. In *Advances in Neural Information Processing Systems*, pp. 1177–1184.
- Ritter, K. (2000). *Average-case analysis of numerical problems*. Number 1733. Springer Science & Business Media.
- Sacks, J., S. B. Schiller, and W. J. Welch (1989). Designs for computer experiments. *Technometrics* 31(1), 41–47.
- Salimbeni, H. and M. Deisenroth (2017). Doubly stochastic variational inference for deep Gaussian processes. In I. Guyon, U. V. Luxburg, S. Bengio, H. Wallach, R. Fergus, S. Vishwanathan, and R. Garnett (Eds.), *Advances in Neural Information Processing Systems*, Volume 30. Curran Associates, Inc.
- Sauer, A., A. Cooper, and R. B. Gramacy (2022a). Vecchia-approximated deep gaussian processes for computer experiments.
- Sauer, A., A. Cooper, and R. B. Gramacy (2022b). Vecchia-approximated deep gaussian processes for computer experiments. *Journal of Computational and Graphical Statistics*, 1–14.
- Sauer, A., R. B. Gramacy, and D. Higdon (2022). Active learning for deep gaussian process surrogates. *Technometrics*, 1–15.

- Schmidt, W. F., M. A. Kraaijveld, and R. P. Duin (1992). Feedforward neural networks with random weights. In *Pattern Recognition, 1992. Vol. II. Conference B: Pattern Recognition Methodology and Systems, Proceedings., 11th IAPR International Conference on*, pp. 1–4. IEEE.
- Sidén, P. and F. Lindsten (2020). Deep Gaussian Markov random fields. In *International Conference on Machine Learning*, pp. 8916–8926. PMLR.
- Stein, M. L. (2014). Limitations on low rank approximations for covariance matrices of spatial data. *Spatial Statistics* 8, 1–19.
- Tran, D., R. Ranganath, and D. M. Blei (2016). The variational Gaussian process. *Proceedings of the International Conference on Learning Representations (ICLR) 2016*.
- van Dam, E. R., B. Husslage, D. den Hertog, and H. Melissen (2007). Maximin Latin hypercube designs in two dimensions. *Oper. Res.* 55(1), 158–169.
- Vecchia, A. V. (1988). Estimation and model identification for continuous spatial processes. *Journal of the Royal Statistical Society: Series B (Methodological)* 50(2), 297–312.
- Wang, W., R. Tuo, and C. F. J. Wu (2020). On prediction properties of kriging: Uniform error bounds and robustness. *J. Amer. Statist. Assoc.* 115(530), 920–930.
- Yang, J. and D. Klabjan (2021). Bayesian active learning for choice models with deep Gaussian processes. *IEEE Transactions on Intelligent Transportation Systems* 22(2), 1080–1092.